Gil Megías, A.; Quintero-Igeño, P.; Mares, A.; Serra, J.; Sánchez-Nevárez, MI.; Miralles, M. (2021). In Silico Hemodynamics and Filtering Evaluation of a Commercial Embolic Protection Device. Annals of Biomedical Engineering. 49(9):2659-2670. https://doi.org/10.1007/s10439-021-02846-4

In silico hemodynamics and filtering evaluation of a commercial embolic protection device

Gil, Antonio[a]; Quintero, Pedro[a]; Mares, Andrea. [a]; Serra, Juan de Ribera [b]; Sánchez-Nevárez, Manuel Ignacio [c]; Miralles, Manuel [c]*

[a] CMT-Motores Térmicos, Universitat Politècnica de València, Camino de Vera, s/n, Valencia, 46022, Spain
[b] Instituto de Restauración del Patrimonio, Universitat Politècnica de València, Camino de Vera, s/n, Valencia, 46022, Spain
[c] Servicio de Angiología y Cirugía Vascular, Hospital Universitario La Fe, Avinguda de Fernando Abril Martorell, 106, Valencia, 46026, Spain
[*]Corresponding author.
E-mail address pedquiig@mot.upv.es (P. Quintero)

Abstract

During the last years, several kinds of Embolic Protection Devices (EPD) have been developed, with the aim of minimizing complication caused by thrombi generated during Carotid Artery Stenting (CAS). These devices are capable of capturing small particles generated during the intervention, avoiding cerebral stroke and improving the outcomes of the surgery. However, they have associated complications, like the increase on flow resistance associated by their use or the lack of knowledge on their actual filtration efficiency for thrombi of low size. Current work proposes a validated computational methodology in order to predict the hemodynamic features and filtering efficiency of a commercial EPD. It will be observed how Computational Fluid Dynamics predicts pressure drop with fair agreement with the experimental measurements. Finally, this work analyzes the filtration efficiency and the influence of the distribution of injected particles on this parameter. The capabilities of the filter for retaining particles of diameter below the pore size is, additionally, discussed.

Total word count: 5960

Keywords: Computational Fluid Dynamics, Embolic Protection Device, Discrete Element Method, Filtration efficiency, Hemodynamics

1. Introduction

Stroke is the second leading cause of death in the world and the leading cause of neurological disability in adults, where up to 20% are due to carotid stenosis [23]. Treatments for carotid stenosis include carotid endarterectomy (CEA) and stent

angioplasty (CAS). Despite the widespread use of CAS, it has been associated with a higher risk of distal embolization with respect to CEA, which could result in greater neurological complications [40]. The emission of particles during CAS is due to the manipulation and fragmentation of the arteriosclerotic plaque. These particles have a varied composition (calcium, fibrin, cholesterol, endothelium, and others), and their size ranges between $10\ \mu m$ and more than $1000\ \mu m$. Particularly, during CAS, it is typically possible to detect up to 100,000 particles smaller than 60 µm, having demonstrated brain damage in animals with sizes of up to 50 µm ([2,10]). Similarly, King and Markus [20] showed that those patients in whom a greater number of microemboli were detected by transcranial Doppler after the procedure had a higher risk of stroke. They showed that 10% of patients with 2 or more microemboli had an annual stroke risk of 15.6%, compared to only 1% of patients in whom no abnormalities were detected ($p < 0.001$).

To minimize this risk, several embolic protection devices (EPD) have been developed and marketed. Among them, the most frequently used are mesh type EPD (mEPD), which are placed distally to the intervention area so that they can filter the released particles [24]. Although its use has improved the results of CAS in terms of reducing ipsilateral stroke and death, a greater number of brain lesions persist compared to CEA, detected by diffusion-weighted magnetic resonance imaging [42]. Furthermore, the hemodynamic resistance they generate has been related to flow obstruction, intolerance and cerebral ischemia [17]. In fact, the inclusion of a carotid mEPD implies a substantial modification of the distal hemodynamics, with the possible appearance of turbulent or low velocity areas, which could result in thrombotic phenomena [35]. Finally, these hemodynamic changes, as well as the filtering efficiency, are explained by structural peculiarities in its design (number of holes, shape of the filter, capability of fitting the whole duct…) and its correct implantation [6] (deviations of the filter during the intervention, favoring particles to escape through the voids created between filter's edge and the wall).

Consequently, to explore the effects of the above parameters on the selection of the most appropriate mEPD, an important amount of research can be found in the literature. These works are mainly based on two different approaches: clinical trials of the devices and in vitro evaluation.

In clinical trials, differences have been suggested in terms of results depending on the type of EPD [9]. Furthermore, there is enough information about EPD complications, such as flow limitation, blockage in the retrieval catheter, vasospasm, poor placement

and emission of embolic particles that seem to depend on the model ([16,17,22]). Despite the undeniable capabilities of this type of analysis, they have the disadvantage of high cost, the need for a large cohort of patients and that the results obtained from their analysis are primary statistics. Therefore, they do not contribute to the physical knowledge of the processes involved during the operation of the mEPD, as they are focused on demonstrating clinical efficacy of the devices.

Regarding the in vitro experimentation, several researchers have detected differences in terms of efficiency and resistance to flow that seem to depend on the design of the device. Siewiorek et al [37] evaluated the filtering efficiency of three mEPD using large polymer microspheres with a diameter between 297 µm and 1000 µm and discovered how more than 92% of the injected particles were correctly trapped. They hypothesized that, despite the greater particle size with respect to the pore, these particles were allowed to escape through the gap created between the filter's edge and the duct wall. This effect was observed for all the tested mEPDs, and would probably increase under in vivo conditions, due to the inclusion of smaller particles, worse positioning of the mEPD and a greater negative effect due to pressure changes. Kurzhals et al [15] carried out a similar study, finding similar results and conclusions. This shows the existence of differences in efficacy and resistance between mEPD, which could be explained by the characteristics of its design([6,26,36,37]), but also by the unproper implantation of the mEPD. Finally, due to experimental difficulties, none of the analyzed works were able to analyze the filtering efficiency, with particles smaller than 50 µm, which could result in possible subsequent ischemic events.

The last methodology that could be applied to understand the behavior of mEPD is the numerical analysis using Computational Fluid Dynamics (CFD). In fact, over the past few years, a great deal of effort has been put into simulating similar medical devices. However, according to the authors' knowledge, the application of CFD for mEPD resistance and efficiency analysis has only been partially explored so far. Therefore, the methodology proposed during this work will be based on similar physical phenomena sharing most of the physics of the system. In this regard, several works can be cited that have successfully applied this methodology in similar physical problems. For instance, Siewiorek and Finol[33] proposed a computational analysis of various EPDs in order to predict their pressure drop, comparing porous media assumption and a direct resolution of EPD holes. However, they did not estimate filtration capabilities of the devices. Louvelle et al [19] showed how CFD simulations could be used to make

hemodynamic predictions in complex situations such as in the study of blood flow efficiency in patients with tetralogy of Fallot repair. On the other hand, Papamanolis et al [27] performed a simulation of myocardial perfusion using a specific patient model. Here, they modelled a complex low-flow rate system with a Newtonian fluid, despite which, they showed sufficiently precise results to model the problem ([7,8,14]). Deyranlou et al [4] used a similar model to estimate aortic circulation and analyze susceptibility to thrombus formation in the aorta and carotid arteries.

Other researchers have focused their analysis on the nature of thrombotic material or its motion during blood circulation to analyze its characteristics. For instance, Johnson et al [13] carried out a review of the multiple existing techniques to predict the aggregation or disaggregation of thrombi, as well as the change of their shape under different loads, making it possible to model the appearance of micro-thrombi from an initial particle. However, the motion of these blood clots was not explored in this reference. In this sense, Mukherjee et al [25] used a Eulerian-Lagrangian methodology to predict the motion of small particles through the circle of Willis and explain how the specific geometry of the patient, size and number of escaped particles could be a crucial factor to develop stroke. Finally, Shadden and Arzani [31] followed the motion of the particles through the pulmonary arteries. Although all these works successfully proposed methodologies for the monitoring of thrombi through the circulatory system, the application of the Lagrangian methodology has not been applied so far to evaluate the performance of mEPD and the possible influence of the interaction between the particles in the results.

The objective of this study is to carry out an in silico evaluation of the hemodynamic alterations and the filtration efficiency of the mEPD Angioguard®RX, previously evaluated by Siewiorek et al [32] by means of an in vitro test consisting of a flow circuit filled with 0.9% saline solution. The resistance of the filter will be evaluated for various values of the inlet flow rate and will be validated with experiments in an in vitro model. The resistance data will then be extrapolated for use in fluids of similar viscosity to blood. Additionally, a Discrete Element Method (DEM) methodology will be applied to analyze the filtration efficiency for a distribution of thrombotic material ranging from 50 µm to 140 µm in diameter.

2. Materials and Methods

2.1 Geometry, computational domain, and mesh

During this study, the geometry of the commercial mEPD Angioguard RX was generated, by means of reverse engineering, using the measurements taken from microscopic visualization. This is a device constructed with a polyurethane conic membrane, with approximately 1100 orifices of $100\ \mu\mathrm{m}$ [36]. The device is fixed by 8 nitinol wires of diameter $D_{wire} \approx 0.18\ \mathrm{mm}$. The maximum diameter of the filter was approximately $D_{DPD} = 5.5\ \mathrm{mm}$, with a length of $L_{DPD} = 6.4\ \mathrm{mm}$, as sketched at Figure 1 (top). From the computational point of view, the filter was placed in the interior of a cylindrical pipe of diameter $D = 5.5\ \mathrm{mm}$ assuming, therefore, a perfect fit between the filter and the channel. Deformations of the device will not be considered during this work, as their influence could be expected to be of second order, similarly as performed by Siewiorek and Finol [33,34]. Consequently, current simulations will not take into account the influence of possible gaps between the device and walls, which has been previously related with a decrease of the filtration efficiency when compared with the size of the orifices [5]. This effect is expected to be highly dependent on the particular conditions of the surgery and therefore, they would not be a direct characterization of the mEPD.

Longitudinal dimensions of the pipe were selected after a domain-independence analysis, in order to ensure that their location did not artificially affect the results, leading to an upstream distance of $L_{up} = 10\ D$ and a downstream distance of $L_{down} = 20\ D$, as sketched at Figure 1 (top).

The geometry was discretized using a polyhedral mesh whose maximum size was set to be $\Delta x_{max} = 350\ \mu\mathrm{m}$. Polyhedral mesh was chosen, as it normally ensures grid independence with fewer elements than tetrahedral meshes [38]. A surface size of $\Delta x_{walls} = 35\ \mu\mathrm{m}$ was used in order to represent domain's walls, while the guides and orifices were refined with a size of $\Delta x_{min} = 5.25\ \mu\mathrm{m}$. Finally, the volume near the mEPD was discretized with small cells of size $\Delta x_{near} = 70\ \mu\mathrm{m}$. With this configuration, a mesh with approximately $N = 16 \cdot 10^6$ elements was generated, which is schematically shown at Figure 1 (bottom). Note that, as the orifices were considered in the model, an important number of cells were needed in order to properly characterize the flow through them. A grid independence study was performed with meshes up to $N = 86 \cdot 10^6$ elements without finding significant discrepancies between computed results.

During the experiment, the channel was created using PVC of thickness 13 mm. Note that, due to the relatively low values of inner pressure and velocities expected in the system, deformations of these walls could be neglected without losing accuracy. It should be noticed that, although at in vivo conditions the compliance would lead to deformations significantly higher, these are expected only to partially influence to the results. In fact, most of the previous analyses on the flow through similar vases tend do not include these effects [19,33]. Moreover, the work of Lee et al, showed how the inclusion of the wall deformation in the carotid artery only provided with slight improvements on the accuracy of the computations, with the drawback of a significative increment on the needed computational resources [18].

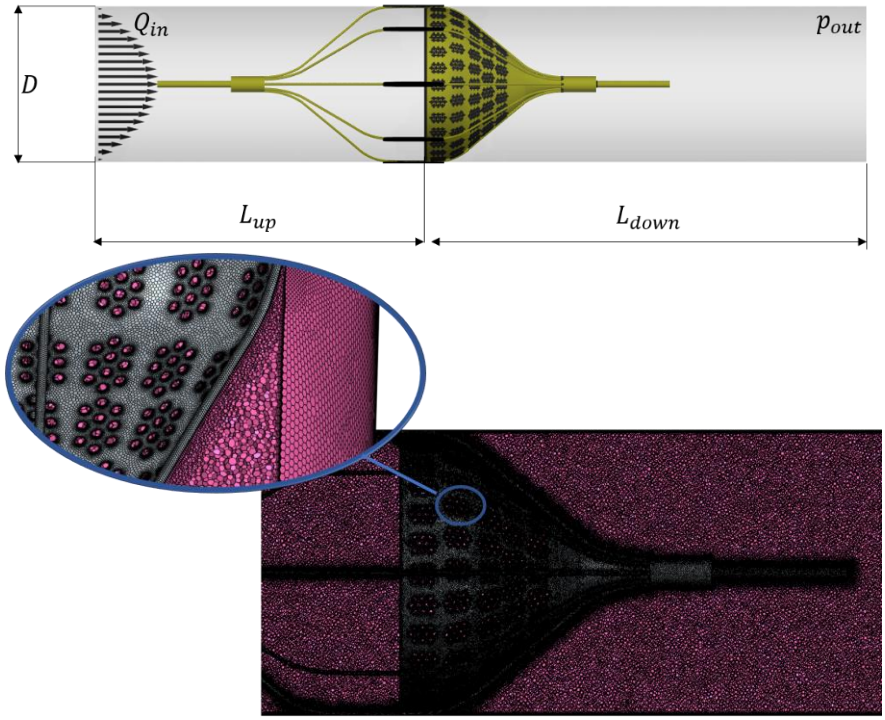

Figure 1 Sketch (not scale) of the geometry (top) and mesh (bottom) of the mEPD

2.2 Boundary conditions

A time-constant laminar volume flow of Q_{in}, ranging between $Q_{in} = 50\ \mathrm{mL\ min^{-1}}$ and $Q_{in} = 650\ \mathrm{mL\ min^{-1}}$ is imposed at the inlet. The incoming flow was set as a fully laminar Poseuille flow, whose spatial velocity profile, $V(r)$, is given by Equation 1, where $V_{ave} = \frac{4\,Q}{\pi\,R^2}$ is the average velocity at the section and r is the radial coordinate at which Equation 1 is evaluated. The fluid was modeled as a saline solution, with density $\rho = 1000\ \mathrm{kg\ m^{-3}}$ and viscosity $\mu = 0.0019\ \mathrm{Pa \cdot s}$. With these assumptions, Reynolds number was varied

between $\mathrm{Re} = \frac{\rho\, V_{ave}\, D}{\mu} = 90$ and $\mathrm{Re} = 1080$, which can be considered to be on the laminar range for pipe flows [30]. Note that, although the incoming flow can be considered to be laminar during the experiment, the presence of the mEPD could generate turbulence downstream.

$$\boldsymbol{V(r) = 2 \cdot V_{ave}} \left(\mathbf{1} - \left(\frac{\mathbf{2\, r}}{\boldsymbol{D}} \right)^{\mathbf{2}} \right) \qquad 1$$

Pressure at the outlet section was constant, with a value of $p = 0\ \mathrm{mmHg}$ (relative to atmospheric pressure). Note that, as walls are considered to be perfectly rigid and the fluid is incompressible, the following results can be applied for any value of the outlet pressure [1].

In order to evaluate the filtering efficiency of the mEPD, four different particle distribution were evaluated, with particle size varying between $50\ \mu\mathrm{m}$ and $140\ \mu\mathrm{m}$. The normalized probability density function (f) and the cumulative density function (F) are shown at Figure 2. Distribution A consisted in a log normal distribution with the mode centered at $D = 70\ \mu\mathrm{m}$, and was designed to evaluate a case in which most of the particles could be considered to be low size thrombi. Distribution B consisted in a reverse log normal distribution with mode centered at $D = 110\ \mu\mathrm{m}$, to model a case in which most of the particles could be considered to be large sized thrombi. Distribution C consisted in a normal distribution with mean at $D_{particle} = 95\ \mu\mathrm{m}$. Finally, a uniform distribution (Distribution D) was considered. Particles were injected upstream the filter at a constant rate of $\dot{N}_{particles} = 5 \cdot 10^5\ \mathrm{particles} \cdot \mathrm{s}^{-1}$ during an injection time of $t_{injection} = 0.02\ \mathrm{s}$, leading to an injection of, approximately, $N_{particles} \approx 10^4$ for all the computations.

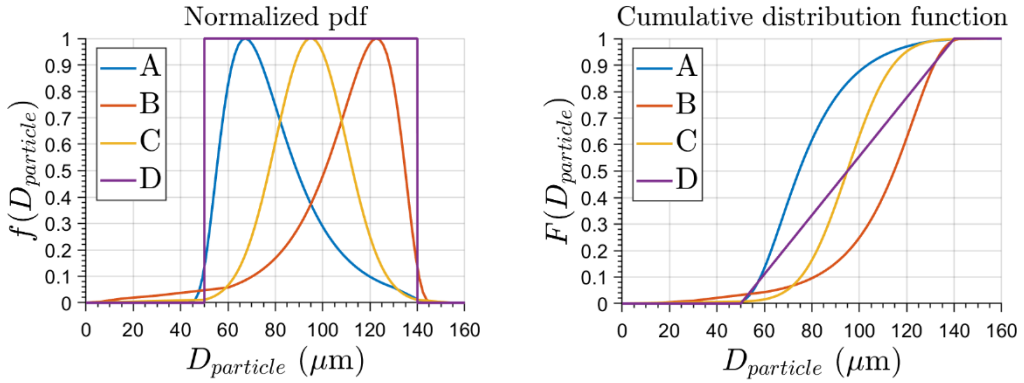

Figure 2 Normalized probability density function (left) and cumulative distribution function (right) of the particles injected during the computations

2.3 CFD-DEM Simulation

Simulations were performed by means of the Finite Volume Method, using the CFD software Simcenter STAR-CCM+ for the resolution of the Reynolds Averaged Navier Stokes (RANS) equations [28]. $k-\omega$ with shear stress transport turbulence model [21] was chosen. This model varies from the $k-\omega$ turbulence model proposed by Wilcox [41] near the walls to the $k-\varepsilon$ model away from them, solving the main inconveniences of both models. Pressure drop was additionally computed assuming laminar flow, with no significative discrepancies. Spatial derivatives were discretized using a second order upwind approach.

The motion of the particles was modeled by means of the Discrete Element Method (DEM), established by *Cundall and Strack* [3] as an extension of the Lagrangian formulation in order to account for inter-particle interaction in the particle equations of motion, which cannot be ignored for highly loaded flows with many interacting particles. DEM particles are modeled based on soft-particle formulation in which particles are allowed to develop an overlap. The calculated contact force is proportional to the overlap, as well as to the particle material and geometric properties. Although DEM was designed for modeling granular flow of complex geometries, during the current work these particles will be assumed to be spherical, with varying values of their diameter, D_p, in order to increase comparability of computations with in vitro analysis. Interaction between particles and walls was modeled using a Hertz-Mindlin approach [29], using typical values for the static friction coefficient $(C_{fs} = 0.61)$, the rolling friction coefficient $(\mu_r = 0.50)$ and tangential restitution coefficient $(C_t = 0.50)$. Equivalent simulations were carried out during the current work for extreme values of these coefficients, without

finding significant discrepancies between the results for spherical particles. Nevertheless, future works should be dedicated in order to obtain these coefficients for the case of embolized plaques of arbitrary shapes. Finally, the equations of motion of the particle are solved using a one-way approach, i.e., the fluid flow is capable to interact with the motion of the particle, but the flow is not substantially affected by the presence of the particles. Consequently, the current analysis will be limited to the analysis of the resistance of the clean filter and its filtering efficiency, which is expected to be the most important parameter for comparing the hemodynamic features of different mEPD.

Finally, reliability of the procedure was ensured by means of application of the norm ASME V&V40 [39]. Particularly, it should be noticed that, the current stage of the analysis (a) model risk is relatively low; (b) a well-established computational code has been used; (c) numerical errors were minimized through a mesh independence analysis and an study of turbulence models; (d) the results analyzed against the comparator under *in vitro* conditions were in a reasonable range of accuracy and (e) comparison of the current results and other similar devices remain on the same order of magnitude. After evaluating these factors, the credibility levels of the proposed methodology ranged from high for the CFD quantifications and medium for the DEM analyses.

2.4 Experimental methodology

The experimental measurements of pressure drop were taken in a closed circuit connected to a study zone with diameter of 5.50 mm in which the mEPD was mounted. The temperature of the measurement zone was kept to approximately 37ºC in order to ensure correct fitting of the device. Current analyses were performed with constant flow using a continuous flow pump BPX-80 Bio-Pump Plus ™ (Medtronic ™), varying the flow rate between $Q_{in} = 150\ \mathrm{mL\,min^{-1}}$ and $Q_{in} = 600\ \mathrm{mL\,min^{-1}}$. The working fluid was a saline dilution, whose density and viscosity were the same than specified during the computational methodology. Pressure was monitored upstream and downstream from the mEPD, in order to obtain measurements of pressure drop using a pressure monitor Spacelabs 90367.

3. Results

3.1 Pressure drop, validation and hemodynamics

As previously stated, the pressure drop through the device is a fundamental parameter in order to perform an evaluation of the suitability of any filtering device, as a large pressure drop induced by the mEPD (large flow resistance) could result into a low flow rate through the carotid and could lead to low cerebral flow rates, which could jeopardize the result of the intervention [11,12].The current work is focused on the evaluation of pressure drop of the device under clean conditions, i.e., before the mEPD is saturated of retained particles. It is expected that, once the filter is saturated, all the mEPD designs should behave similarly, producing a significant flow resistance and decreasing cerebral perfusion. Figure 3 (left) shows the comparison between the computed values of pressure drop and the experimental measurements, indicating a fair agreement of the computational methodology. Additionally, the values of pressure drop of Siewiorek and Finol [33] are represented in the Figure. Note how pressure drop of Angioguard™ is of the same order of similar devices, like Emboshield and Accunet.

Note how, although it can be observed that pressure tends to increase with the value of volume flow rate, this increment is not completely quadratic, indicating that Reynolds number plays an important role for computing pressure drop. In fact, dimensional analysis should be applied for extrapolating computed pressure drop for more viscous fluids, like blood. Figure 3 (right) shows the value of pressure drop coefficient $\left(\Delta c_p = \frac{\Delta p}{\frac{1}{2}\rho V_\infty^2}\right)$, which is a function only of the Reynolds number. Note how this non-dimensionalization could be applied in order to infer actual value of flow resistance for other fluids (like blood at various values of hematocrit) or different sizes of the device. In fact, it was found that Δc_p for Angioguard device could be estimated by the regression stated at Equation 2.

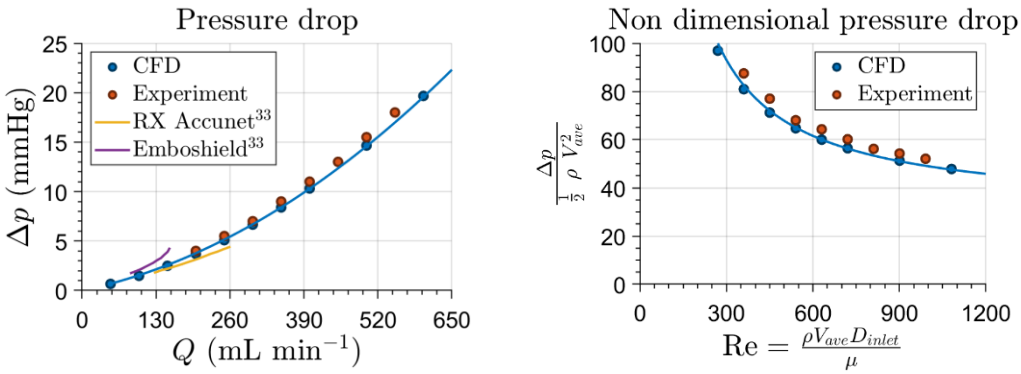

Figure 3 Experimental and computational pressure drop (left) for a fluid of $\mu = 0.0019$ Pa s and $\rho = 1000$ kg m^{-3}. Non-dimensional pressure drop as a function of Reynolds number (right). Comparison of the results for similar devices, extracted from Siewiorek and Finol [33]

$$\boldsymbol{\Delta c_p = \Delta c_{p0} + \frac{K}{\mathrm{Re}}} \qquad 2$$

Where the constants were estimated to be $\Delta c_{p0} = 30$ and $K = 1.90 \cdot 10^4$ for the actual computation.

Pressure drop through a mEPD is related with the hemodynamics of the flow when passing through. In this sense, it is possible to analyze both velocity and pressure fields in the interior of the duct. Figure 4 shows longitudinal and transverse sections of the flow for a particular value of $Q_{in} = 300\,\mathrm{mL\,min^{-1}}$. Note how pressure drop experiences an abrupt decrease, which is mainly due to the low effective section conformed by the small orifices. Additionally, it can be observed an important recirculation zone downstream the device, which could be a possible distal thrombi generation area. Both the high maximum velocities and the existence of these large recirculation are the cause of the large pressure drop experienced by the Angioguard™ mEPD. An increase of the size of the orifices would lead to a lower value of pressure drop. However, these design guidelines would act against filtration efficiency at large sizes and, consequently, a careful trade-off between these should be reached.

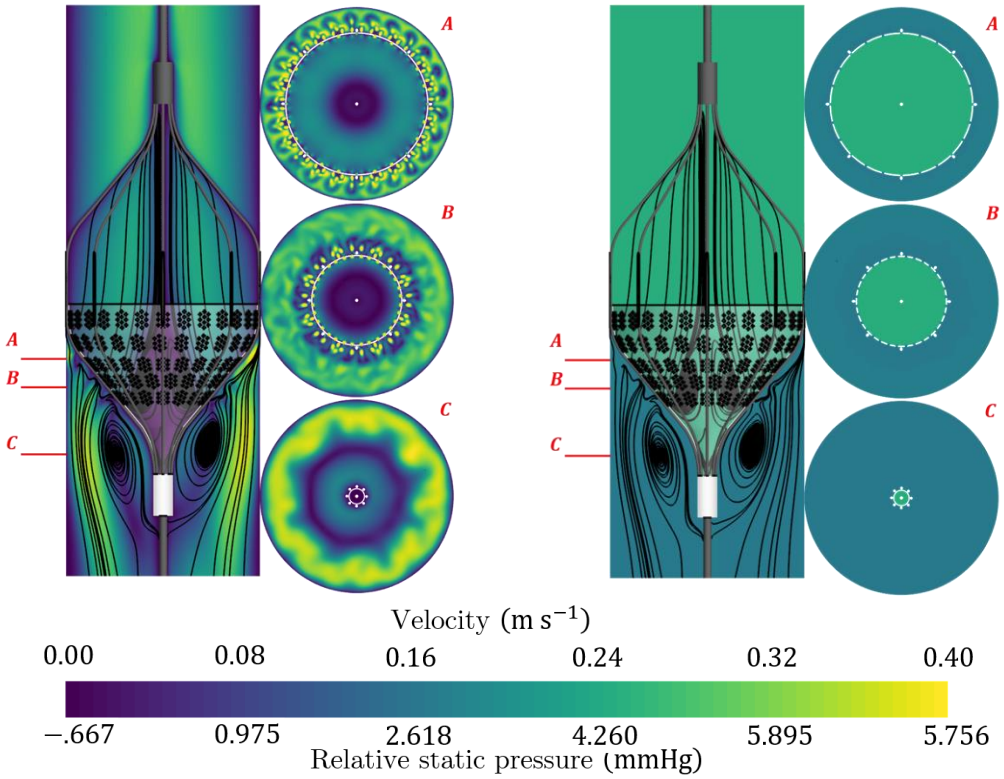

Figure 4 Velocity (left) and pressure fields (right) at a longitudinal section and at different transversal sections for a saline dilution at $Q_{in} = 300\ \mathrm{mL\ min^{-1}}$

Figure 4 allows, additionally, to observe how the pressure distribution is approximately uniform for each transversal section, while the velocity field shows the greatest variation. Note the high values of velocity (yellow colors observed at sections A and B) at orifices and how the flow is detached after them (dark blue zones at sections A and B). Additionally, at section C, the effective section is substantially reduced, indicating high speed zones, responsible of high pressure drops in combination with a recirculation zone, responsible of higher probability of thrombi generation.

3.2 Filtering efficiency

In order to evaluate the filtering efficiency of the mEPD, different distribution of spherical particles were injected, as described during section 2.1. The number of particles resident in the computational domain was followed during the whole simulation, allowing to evaluate which particles were trapped by the device. During this section, calculations are focused for the case of $Q_{in} = 300\ \mathrm{mL\ min^{-1}}$. Additional simulations were performed for other values of volume flow rate, although they are not

shown for reasons of brevity. Figure 5 (left) shows the number of resident particles in the domain during the simulated time. Note how they tend asymptotically to a constant value, indicating steady system. Note how the number of particles trapped by the system ranges from a 63% for distribution A to a 96% for distribution B, which is mainly due to the differences between particles size injected at each case. This can be confirmed by Figure 5 (right) in which the number of particles of diameter below $90\mu\text{m}$ is shown for the same calculations. However, observation of Figure 5 (right) allows to deduce that, for the current case, filtration efficiency is not a function only of the particle diameter, but also on the own considered injection distribution, as will be later discussed.

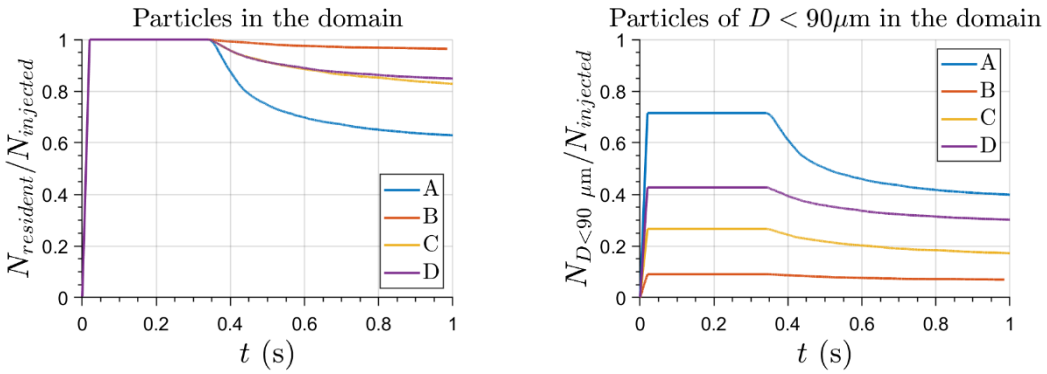

Figure 5 Resident particles in the interior of the fluid domain (left) and resident particles of $D < 90\ \mu\text{m}$ in the interior of the domain (right) during a whole calculation with saline dilution at $Q_{in} = 300\ \text{mL min}^{-1}$

In order to obtain larger insight on how particles of different diameter are filtered during the current simulations, Figure 6 shows the particle distribution of injected particles (blue) and the particles which are retained after a sufficiently large simulation time (orange). Note how, as it could be expected, filtration efficiency is of 100% for particles whose size is larger than the orifices' diameter $(90\ \mu\text{m})$. This is in accordance with previous research, which concluded that lack of efficiency at large particles of this kind of filters could only be attributed to the lack of fitting of the mEPD to the duct [5], which is not being considered during this work. Future efforts will be dedicated in order to provide with a full quantification of these phenomena. Additionally, mEPD offers an important filtration effect for particles whose size is lower than orifices' diameter. However, for these particles, the filtration efficiency is highly dependent of the own injected distribution. For instance, for distribution at which low size particles are

dominant, like distribution A, a 63% of the particles of $80\mu m$ are retained by the mEPD. This value is significantly higher for distributions B and D, (85% and 82%, respectively), characterized by a larger size of the injected particles. This effect of the injected distribution on the filter efficiency is even more noticeable for particles of lower size: while 56% of the particles of $60\mu m$ are trapped when Distribution A is injected, this parameter reaches values of almost 80% for Distribution B.

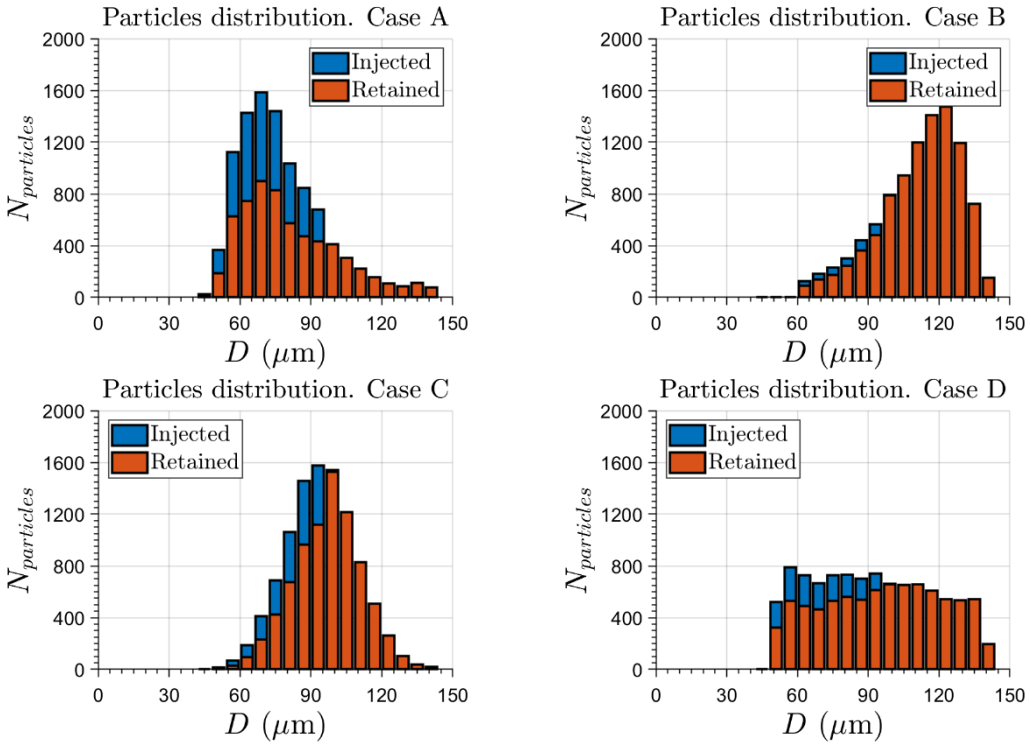

Figure 6 Distribution of the particles injected in the domain (blue) and particles retained by the filter after stabilization (orange) for the different injection cases

As it has been explained, functioning of the device is highly dependent on the device. Therefore, in order to understand the influence of the distribution on the filtering efficiency of the device, Figure 7 shows the evolution of the particles during the simulation for a case in which low size particles are dominant (Distribution A) and other dominated by the effect of large particles (Distribution B). Note how, when the particles reach the mEPD ($t = 0.06\ s$), an important amount of low size particles are capable to escape through the orifices for Distribution A. This is slightly different for distribution B. At this case observe how, although some low size particles are leaving the mEPD, the effect of large particles act as a blockage, increasing filtration efficiency for low size particles. Note that, additionally, when the filter is saturated, flow resistance of

mEPD will be increased, although this was not modeled during the current work.
365 Finally, observe how small particles remain at the recirculation zone of the filter during a noticeable time snap after they abandon the mEPD. This should be carefully thought during future redesigns of the device, as this particles at a recirculation zone could act as a distal thrombi generation nucleus.

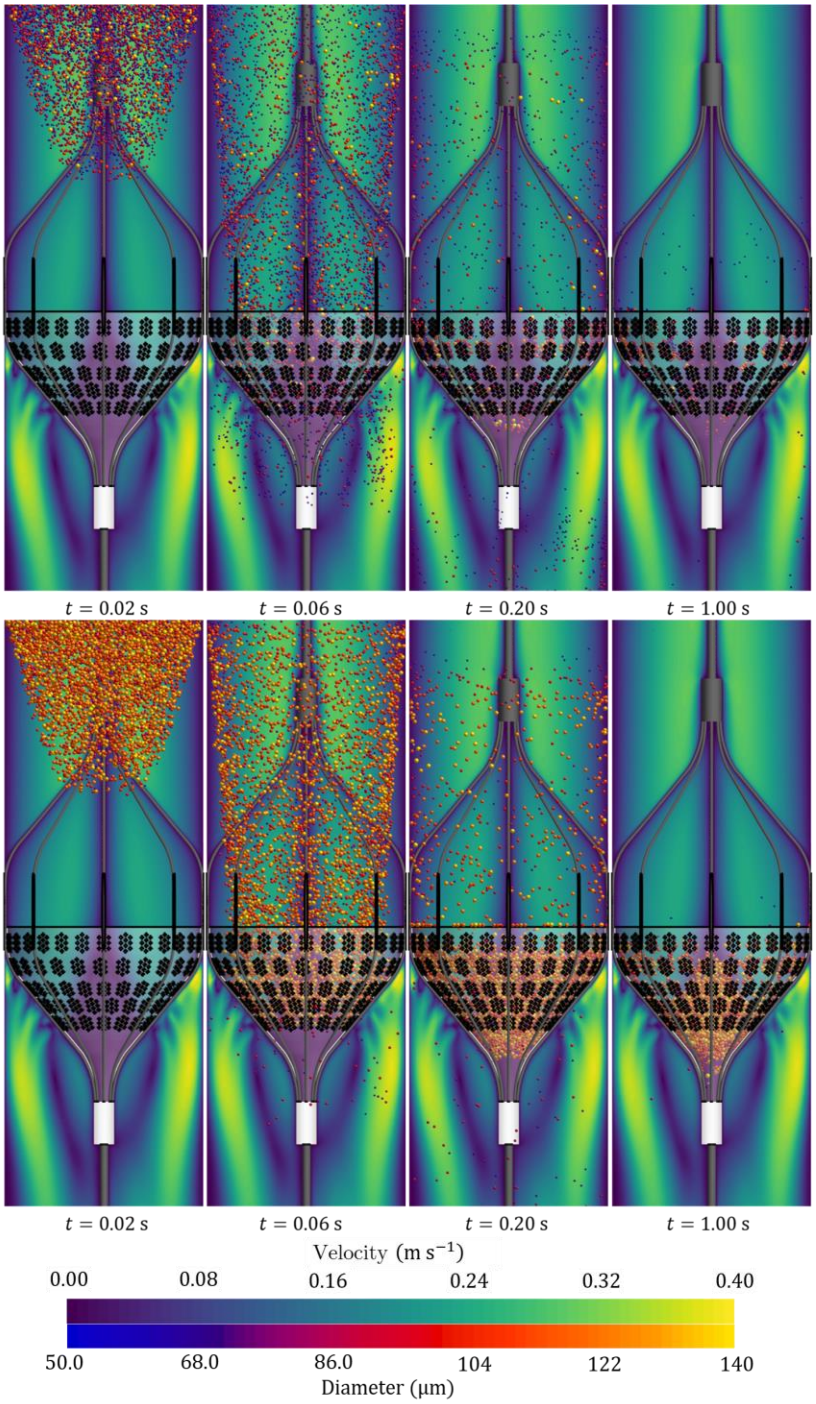

Figure 7 Evolution of particle's motion for distribution A (top) and B (bottom) at different time steps for $Q_{in} = 300$ mL min^{-1} and saline dilution as the working fluid

The filter efficiency η_X is additionally represented at Figure 8, defined, as stated by Equation **3,** as the ratio of the number of retained particles whose diameter is greater than X and the number with $D > X$ which were injected in the domain, as a function of the diameter of the filtered particle and the injection distribution.

$$\boldsymbol{\eta_X = \frac{N_{retained,D>X}}{N_{injected,D>X}}} \qquad 3$$

Figure 8 (left), allows to observe the already discussed influence of the large particles on the filter efficiency, showing significative discrepancies on the filtration efficiency for Distributions A and B. On the other hand, Figure 8 (right) allows to provide an additional visualization of how the interaction between particles acts as an additional filtration mechanism. In fact, at Figure 8 (right, A) and Figure 8 (right, B) it is possible to observe how large particles, or a combination of small particles tend to occlude orifices. When this is the case, the rest of the particle will collide with them and will tend to form a cluster of particles, leading to an almost absolute efficiency of the orifice. However, it should be considered that, when this is the case the flow resistance of the mEPD will be significantly increased, although it was not quantified during this work. Finally, Figure 8 (right, C) shows how small particles are also retained at the bottom of the mEPD, explaining filtration efficiency of low size particles even for particles of size below orifices' diameter. Observe also how a significant amount of particles tend to be accumulated at the edge of the mEPD, which helps to explain why experimental research has previously shown escaped particles when fitting is not perfect [5] or when the filter is extracted [15].

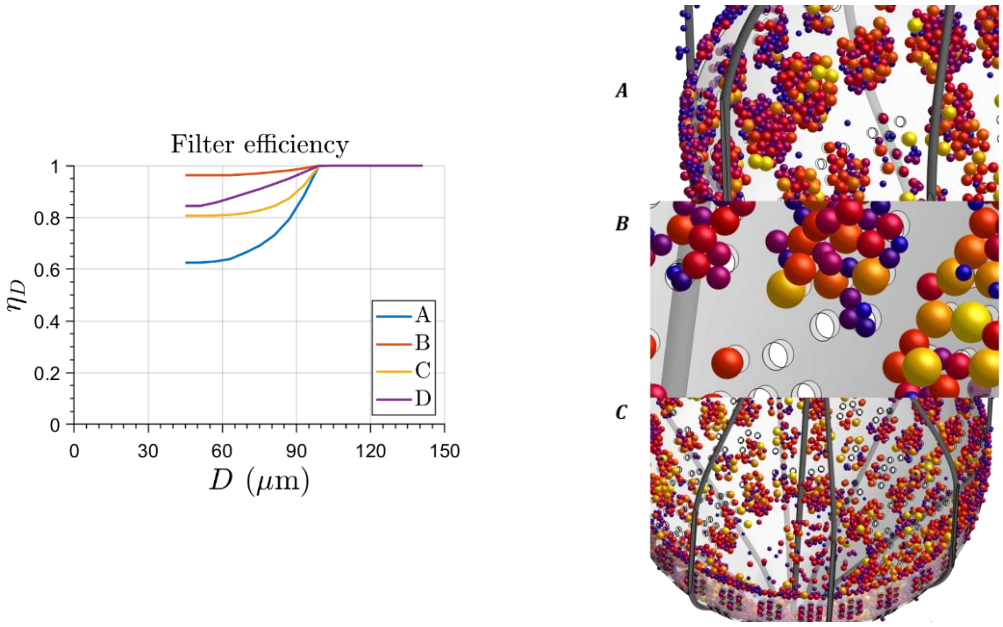

Figure 8 Resident particles in the interior of the fluid domain (left) and resident particles of $D < 90\ \mu m$ in the interior of the domain (right) during a whole calculation with saline dilution at $Q_{in} = 300\ mL\ min^{-1}$

4. Discussion

During this work, the commercial device Angioguard ™ has been explored by means of an *in vitro* experiment and *in silico* analysis, using computational fluid dynamics. By comparing the flow resistance of the computational calculations and the experimental measurements, it has been observed how the former can predict accurately this parameter, validating the methodology. It has been observed that pressure drop is highly dependent on Reynolds number and, therefore, the analysis performed using a saline dilution should be carefully used. Consequently, a non-dimensional representation of the pressure drop has been deduced, allowing physicians to accurately predict the decrease on cerebral irrigation when installing the mEPD, including the effect of blood viscosity at any value of hematocrit. Current results did not include the effect of filter saturation for computing the increase on flow resistance. Future efforts should be dedicated in order to perform 2-way coupled simulations and account for how obstruction of the orifices would cause significative decrease on the flow rate for a given pressure drop.

Additionally, current work analyzed the effect of the kind of particle distribution on the own filter efficiency and showed how the different mechanisms of filtering are affected for distributions with large and small particles. It was observed how the effect

of particle interaction should be considered for an accurate estimation of the filter efficiency and how Angioguard ™ is capable to capture more than 60% of particles with $D > 60\,\mu\mathrm{m}$, which should be beneficial in order to improve the results of the intervention.

Finally, current work has been useful in order to improve the knowledge of the hemodynamics in the interior of Angioguard ™ mEPD and it could be used for future works in order to improve the outcomes of this kind of devices. For instance, it has been observed how particles tend to accumulate at the peripheric of the device, explaining the important lack of efficiency during explantation of the mEPD. Future designs should consider this fact in order to force particles to accumulate in a safety zone of the mEPD, especially at its inferior part. It has also been observed how an important recirculation zone was generated downstream the mEPD, which could be responsible of distal thrombi generation. Future efforts will be dedicated to proposing new designs which could avoid this kind of phenomena.

Finally, it should be noticed that, although the flow has been considered to be steady and Reynolds number is low, these zones of flow recirculation are susceptible of be nuclei of turbulence generation and, therefore, future efforts will be dedicated in order to quantify possible turbulent unsteady effects using scale resolving simulations

References

1. Anderson Jr, J. D. Fundamental of Aerodynamics. McGraw-Hill Education, 2010.
2. Coggia, M., O. Goëau-Brissonnière, J. L. Duval, J. P. Leschi, M. Letort, and M. D. Nagel. Embolic risk of the different stages of carotid bifurcation balloon angioplasty: An experimental study. *Journal of Vascular Surgery* 31:550–557, 2000.
3. Cundall, P. A., and O. D. L. Strack. A discrete numerical model for granular assemblies. *Géotechnique* 29:47–65, 1979.
4. Deyranlou, A., J. H. Naish, C. A. Miller, A. Revell, and A. Keshmiri. Numerical Study of Atrial Fibrillation Effects on Flow Distribution in Aortic Circulation. *Annals of Biomedical Engineering* 48:1–18, 2020.
5. Finol, E. A., C. M. Scotti, I. Verdinelli, C. H. Amon, and M. H. Wholey. Performance assessment of embolic protection filters for carotid artery stenting. *Modelling in Medicine and Biology VI* 1:133–142, 2005.
6. Finol, E. A., G. M. Siewiorek, C. M. Scotti, M. H. M. H. Wholey, and M. H. M. H. Wholey. Wall apposition assessment and performance comparison of distal protection filters. *Journal of*

Endovascular Therapy 15:177–185, 2008.

7. Graf, C., and J. P. Barras. Rheological properties of human blood plasma - A comparison of measurements with three different viscometers. *Experientia* 35:224–225, 1979.

8. Haidekker, M. A., A. G. Tsai, T. Brady, H. Y. Stevens, J. A. Frangos, E. Theodorakis, and M. Intaglietta. A novel approach to blood plasma viscosity measurement using fluorescent molecular rotors. *American Journal of Physiology-Heart and Circulatory Physiology* 282:H1609–H1614, 2002.

9. Hart, J. P., P. Peeters, J. Verbist, K. Deloose, and M. Bosiers. Do device characteristics impact outcome in carotid artery stenting? *Journal of Vascular Surgery* 44:725–730, 2006.

10. Heistad, D. D., M. L. Marcus, and S. Mueller. Measurement of Cerebral Blood Flow With Microspheres. *Archives of Neurology* 34:657–659, 1977.

11. Hendriks, J. M., J. D. Zindler, A. Van Der Lugt, P. M. T. Pattynama, M. R. H. M. Van Sambeek, J. L. Bosch, and L. C. Van Dijk. Embolic protection filters for carotid stenting: Differences in flow obstruction depending on filter construction. *Journal of Endovascular Therapy* 13:47–50, 2006.

12. Howell, M., Z. Krajcer, K. Dougherty, N. Strickman, M. Skolkin, B. Toombs, and D. Paniagua. Correlation of Periprocedural Systolic Blood Pressure Changes with Neurological Events in High-Risk Carotid Stent Patients. *Journal of Endovascular Therapy* 9:810–816, 2002.

13. Johnson, S., S. Duffy, G. Gunning, M. Gilvarry, J. P. McGarry, and P. E. McHugh. Review of Mechanical Testing and Modelling of Thrombus Material for Vascular Implant and Device Design. *Annals of Biomedical Engineering* 45:2494–2508, 2017.

14. Karimi, S., M. Dabagh, P. Vasava, M. Dadvar, B. Dabir, and P. Jalali. Effect of rheological models on the hemodynamics within human aorta: CFD study on CT image-based geometry. *Journal of Non-Newtonian Fluid Mechanics* 207:42–52, 2014.

15. Kurzhals, A., J. B. Matthies, R. Andresen, C. Wissgott, K. P. Schmitz, N. Grabow, and W. Schmidt. Efficiency test of current carotid embolic protection devices. *Biomedizinische Technik* 62:349–355, 2017.

16. Kwon, B. J., M. H. Han, H. S. Kang, and C. Jung. Protection filter-related events in extracranial carotid artery stenting: A single-center experience. *Journal of Endovascular Therapy* 13:711–722, 2006.

17. Kwon, O. K., S. H. Kim, E. A. Jacobsen, and M. P. Marks. Clinical implications of internal carotid artery flow impairment caused by filter occlusion during carotid artery stenting. *American Journal of Neuroradiology* 33:494–499, 2012.

18. Lee, S. H., S. Kang, N. Hur, and S.-K. Jeong. A fluid-structure interaction analysis on hemodynamics in carotid artery based on patient-specific clinical data †. *Journal of Mechanical Science and Technology* 26:3821–3831, 2012.

19. Louvelle, L., M. Doyle, G. Van Arsdell, C. Amon, G. Van Arsdell, and C. Amon. The Effect of

Geometric and Hemodynamic Parameters on Blood Flow Efficiency in Repaired Tetralogy of Fallot Patients. *Annals of Biomedical Engineering* 1–14, 2021.doi:10.1007/s10439-021-02771-6

20. Markus, H. S., A. King, M. Shipley, R. Topakian, M. Cullinane, S. Reihill, N. M. Bornstein, and A. Schaafsma. Asymptomatic embolisation for prediction of stroke in the Asymptomatic Carotid Emboli Study (ACES): a prospective observational study. *The Lancet Neurology* 9:663–671, 2010.

21. Menter, F. R. Zonal two equation κ-ω turbulence models for aerodynamic flows. *AIAA 23rd Fluid Dynamics, Plasmadynamics, and Lasers Conference, 1993* , 1993.

22. Montorsi, P., L. Caputi, S. Galli, E. Ciceri, G. Ballerini, M. Agrifoglio, P. Ravagnani, D. Trabattoni, G. Pontone, F. Fabbiocchi, A. Loaldi, E. Parati, D. Andreini, F. Veglia, and A. L. Bartorelli. Microembolization during carotid artery stenting in patients with high-risk, lipid-rich plaque: A randomized trial of proximal versus distal cerebral protection. *Journal of the American College of Cardiology* 58:1656–1663, 2011.

23. Morris, D. R., K. Ayabe, T. Inoue, N. Sakai, R. Bulbulia, A. Halliday, and S. Goto. Evidence-Based Carotid Interventions for Stroke Prevention: State-of-the-art Review. *J Atheroscler Thromb* 24:0–000, 2017.

24. Mousa, A. Y., J. E. Campbell, A. F. Aburahma, and M. C. Bates. Current update of cerebral embolic protection devices. *Journal of Vascular Surgery* 56:1429–1437, 2012.

25. Mukherjee, D., N. D. Jani, J. Narvid, and S. C. Shadden. The Role of Circle of Willis Anatomy Variations in Cardio-embolic Stroke: A Patient-Specific Simulation Based Study. *Annals of Biomedical Engineering* 46:1128–1145, 2018.

26. Nevárez, M. I. S., E. P. Andani, and M. M. Hernández. Hemodynamic impact analysis of mesh-type embolic protection devices in an in vitro model. *Angiologia* 72:178–185, 2020.

27. Papamanolis, L., H. J. Kim, C. Jaquet, M. Sinclair, M. Schaap, I. Danad, P. van Diemen, P. Knaapen, L. Najman, H. Talbot, C. A. Taylor, and I. Vignon-Clementel. Myocardial Perfusion Simulation for Coronary Artery Disease: A Coupled Patient-Specific Multiscale Model. *Annals of Biomedical Engineering* 49:1432–1447, 2021.

28. Pope, S. B. Turbulent flows. Cambridge, 2012.

29. Di Renzo, A., and F. P. Di Maio. Comparison of contact-force models for the simulation of collisions in DEM-based granular flow codes. *Chemical Engineering Science* 59:525–541, 2004.

30. Ryan, N. W., and M. M. Johnson. Transistion from laminar to turbulent flow in pipes. *AIChE Journal* 5:433–435, 1959.

31. Shadden, S. C., and A. Arzani. Lagrangian Postprocessing of Computational Hemodynamics. *Annals of Biomedical Engineering* 43:41–58, 2014.

32. Siewiorek, G. M., M. K. Eskandari, and E. A. Finol. The Angioguard™ embolic protection device.

Expert Review of Medical Devices 5:287–296, 2008.

33. Siewiorek, G. M., and E. A. Finol. Computational Modeling of Distal Protection Filters: *http://dx.doi.org/10.1583/10-3178.1* 17:777–788, 2010.

34. Siewiorek, G. M., and E. A. Finol. Experimental and Computational Evaluation of Embolic Protection. *ASME 2010 Summer Bioengineering Conference, SBC 2010* 627–628, 2013.doi:10.1115/SBC2010-19693

35. Siewiorek, G. M., R. T. Krafty, M. H. Wholey, and E. A. Finol. The association of clinical variables and filter design with carotid artery stenting thirty-day outcome. *European Journal of Vascular and Endovascular Surgery* 42:282–291, 2011.

36. Siewiorek, G. M., M. H. Wholey, and E. A. Finol. Vascular Resistance in the Carotid Artery: An In Vitro Investigation of Embolic Protection Filters. *Journal of Vascular and Interventional Radiology* 19:1467–1476, 2008.

37. Siewiorek, G. M., M. H. Wholey, and E. A. Finol. In vitro performance assessment of distal protection filters: Pulsatile flow conditions. *Journal of Endovascular Therapy* 16:735–743, 2009.

38. Spiegel, M., T. Redel, J. J. Zhang, T. Struffert, J. Hornegger, R. G. Grossman, A. Doerfler, and C. Karmonik. Tetrahedral vs. polyhedral mesh size evaluation on flow velocity and wall shear stress for cerebral hemodynamic simulation. *Computer Methods in Biomechanics and Biomedical Engineering* 14:9–22, 2011.

39. The American Society of Mechanical Engineers. V&V 40-2018 Assessing Credibility of Computational Modeling Through Verification and Validation: Application to Medical Devices. 2018.

40. Traenka, C., S. T. Engelter, M. M. Brown, J. Dobson, C. Frost, and L. H. Bonati. Silent brain infarcts on diffusion-weighted imaging after carotid revascularisation: A surrogate outcome measure for procedural stroke? A systematic review and meta-analysis. *European Stroke Journal* 4:127–143, 2019.

41. Wilcox, D. C. Multiscale model for turbulent flows. *AIAA Journal* 26:1311–1320, 1988.

42. Zhou, W., B. D. Baughman, S. Soman, M. Wintermark, L. C. Lazzeroni, E. Hitchner, J. Bhat, and A. Rosen. Volume of subclinical embolic infarct correlates to long-term cognitive changes after carotid revascularization. *Journal of Vascular Surgery* 65:686–694, 2017.